ChemComm

COMMUNICATION

View Article Online
View Journal | View Issue

Cite this: *Chem. Commun.*, 2024, **60**, 304

Received 3rd October 2023,
Accepted 30th November 2023

DOI: 10.1039/d3cc04899c

rsc.li/chemcomm

Mixed-magnesium/zinc calix[4]arene complexes: structure, and ring opening polymerisation studies†

Henry J. S. Banks,[a] Josef W. A. Frese,[a] Mark R. J. Elsegood [a] and Carl Redshaw *[b]

Different combinations of organomagnesium reagents and zinc bromide react with either 1,3-dimethoxy-4-*tert*-butylcalix[4]areneH$_2$ (L(OMe)$_2$H$_2$) or trialkoxycalix[4]arenes (L(OR)$_3$H) (R = *n*-Pr, *n*-pentyl) to afford mixed-metal calix[4]arene systems. Intriguing molecular structures are formed and the systems are capable of the ring opening polymerisation of ε-caprolactone under N$_2$, air, or as melts.

Given the current environmental issues associated with petroleum-derived plastics, there is a drive to develop alternative products.[1] One possibility receiving much attention is the ring opening polymerisation (ROP) of cyclic esters, which can be catalyzed by a variety of species (organic or inorganic).[2] For metal-catalyzed systems, coordination chemistry can play a crucial role in the development of new biopolymers with desirable features, given that control over metal ligation allows for control over polymer properties. The choice of metal is dictated by a number of factors including activity, abundance, cost, and toxicity. The use of earth-abundant metals is particularly attractive, and of these, both magnesium (8th most abundant) and zinc (24th most abundant) have attracted considerable attention in ROP systems.[2d,g,h]

In terms of ancillary ligands, calix[*n*]arenes continue to attract interest, driven in part by their facile functionalisation as well as a tendency to form highly crystalline products.[3] With this in mind, we were attracted by the ability of calixarenes to bind to multiple centres; also, reported calixarene toxicity profiles suggest they are suitable scaffolds.[4] Although the larger calix[*n*]arenes ($n \geq 6$) can accommodate multiple metals by virtue of their conformational flexibility,[5] for calix[4]arenes, the tendency is to bind to one metal and adopt a cone conformation.[3] However, there are a handful of examples in which calix[4]arene has been shown to bind to more than one metal centre,[3,6] whilst mixed-metal calixarene complexes are limited to Fe_2Ln_2 *p-tert*-butylcalix[4]arene clusters (Ln = lanthanide),[7a] MNi_4 (M = Mn, Co, Cu) *p-tert*-butylthiacalix[6]arene clusters,[7b] and group V/VI (Nb or Ta with V or W).[7c] Moreover, we note that for ROP, the use of heterometallic catalysts is a relatively new area,[8] whilst polymetallic systems are also attracting attention.[9] Additionally, given only limited work has been reported using calixarenes for ROP,[3,10] this encouraged us to target multi-metallic calix[4]arene-based catalysts incorporating mixed-metal systems. Herein, we report the molecular structures of products arising from reactions of organomagnesium reagents and Br_2Zn with di- and trialkoxycalix[4]arenes.

Our initial entry into such systems involved the *in situ* reaction of the Grignard reagent $C_6F_5C_6F_4MgBr$[11] with $BF_3{\cdot}Et_2O$, followed by addition of $ZnMe_2$, and then 1,3-dimethoxy-4-*tert*-butylcalix[4]arene (L(OMe)$_2$H$_2$) in the presence of K_2CO_3. Following work-up (MeCN), a white crystalline product was isolated. The molecular structure is shown in Fig. 1 (for alternative views and packing see Fig. S1–S3, ESI†); selected bond lengths and angles are given in the caption. The formula is $\{Mg(NCMe)_2[ZnX_2(NCMe)]_2L(OMe)_2\}{\cdot}1.5MeCN$ (**1**·1.5MeCN), {X = $Br_{1.47}Cl_{0.53}$} with two metal complexes and three MeCNs of crystallisation in the asymmetric unit. There was a low level of chloride contamination in the bromide starting materials. Interestingly here, in addition to the central distorted octahedral Mg centre, there are X_2Zn groups present at the 2,4-positions of the calix[4]arene lower-rim. We have previously noted the formation of bound Br_2Zn fragments on addition of $ZnEt_2$ to a cobalt bromide complex.[12] In **1**, the magnesium ion coordinates to the four calixarene oxygens and additionally to two *trans* NCMe ligands to give an octahedral geometry. One of these NCMe ligands occupies the calixarene cavity. The non-methylated calixarene oxygens additionally bond to one tetrahedral zinc ion each, with the latter additionally binding to two

[a] *Chemistry Department, Loughborough University, Loughborough, Leicestershire, LE11 3TU, UK*
[b] *Plastics Collaboratory, Chemistry, School of Natural Sciences, University of Hull, Cottingham Road, Hull, HU6 7RX, UK. E-mail: c.redshaw@hull.ac.uk*

† Electronic supplementary information (ESI) available: Synthetic details for **1–4**; alternative views of **1–4**; crystallographic and ROP data. CCDC 2298247–2298250. For ESI and crystallographic data in CIF or other electronic format see DOI: https://doi.org/10.1039/d3cc04899c

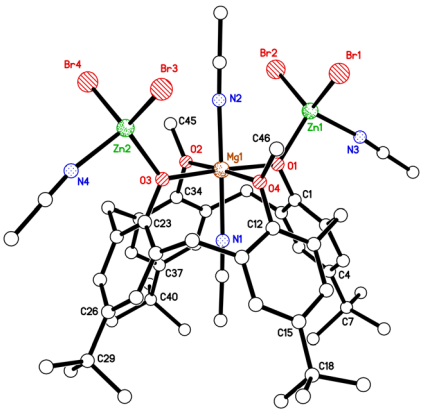

Fig. 1 Molecular structure of one of two similar molecules of $\{Mg(NCMe)_2[ZnX_2(NCMe)]_2L(OMe)_2\}\cdot 1.5MeCN$ (**1**·1.5MeCN) in the asymmetric unit. Selected bond lengths (Å) and angles (°): Mg(1)–O(1) 2.029(3), Mg(1)–O(2) 2.111(3), Mg(1)–O(3) 2.038(2), Mg(1)–O(4) 2.123(3), Mg(1)–N(1) 2.185(3), Zn(1)–O(1) 1.977(2), Zn(1)–Br(1) 2.3409(8), Zn(1)–Br(2) 2.3548(7), Zn(1)–N(3) 2.071(4), O(1)–Mg(1)–O(2) 90.98(10), O(1)–Mg(1)–O(3) 177.08(11), N(1)–Mg(1)–N(2) 179.33(14), Mg(1)–O(1)–Zn(1) 126.17(12). H atoms & minor disorder components omitted.

halide ions and an NCMe ligand. The Mg–O bonds to the phenolate calixarene oxygens are significantly shorter than those to the methylated oxygens. One calixarene has an almost symmetrical cone conformation, while the other has a slightly pinched-cone conformation: C(4)···C(26) = 7.941(5) Å, C(15)···C(37) = 7.971(5) Å, C(50)···C(72) = 8.150(5) Å, C(61)···C(83) = 7.744(5) Å.

Given the presence of the X_2Zn groups in **1**·1.5MeCN, we then targeted a mixed Mg/Zn species directly *via* the use of Br_2Zn as a reagent. Interaction of L(O*n*-Pr)$_3$H with Mg(*n*-Bu)$_2$ and subsequently Br_2Zn afforded, following work-up (MeCN), the complex $[(ZnBr(NCMe)][XZn(\mu\text{-}X)ZnX](\mu^3\text{-}OH)_2[Mg(MeCN)L(O\textit{n}\text{-}Pr)]_2\cdot 5.19MeCN$, **2**·5.19MeCN. {X is again a mixture: $Br_{2.42}Cl_{0.58}$} The molecular structure is shown in Fig. 2 (and Fig. S4, ESI†) with selected bond lengths and angles given in the caption. The asymmetric unit contains one metallocalix[4]arene complex and *ca.* 5.2 acetonitrile molecules. The equivalent Mg sites are six coordinate and octahedral while the Zn sites are four coordinate and tetrahedral except for Zn(3) which is 5 coordinate and TBP (τ = 0.88).[13] The Zn sites bear the Br/Cl ligands, three of which are terminal, the other bridging two zincs. The hydroxo O(10) bridges both magnesium centres and one zinc. The magnesium centres additionally coordinate to three phenolates, the O*n*-Pr, and one MeCN which resides in the calixarene cone. There are three different Zn environments, with Zn(1) and Zn(2) centres binding to two halides (one terminal, one bridging), a hydroxo which bridges them {O(9)}, and a phenolate O. Zn(3) binds to two phenolates, both hydroxos and a MeCN, while Zn(4) binds to two phenolates, a terminal bromide and a MeCN. In terms of charge, the 6 metal sites give 12+, which is balanced by two calixarenes (each is 3−), four halides and two hydroxos. The hydroxo at O(10) forms an intramolecular H-bond with Br(3). In the packing of **2**, the hydroxo at O(9) forms an H-bond with the MeCN of crystallisation containing N(5). There are also some other weak C–H···N/X interactions linking neighbouring molecules together.

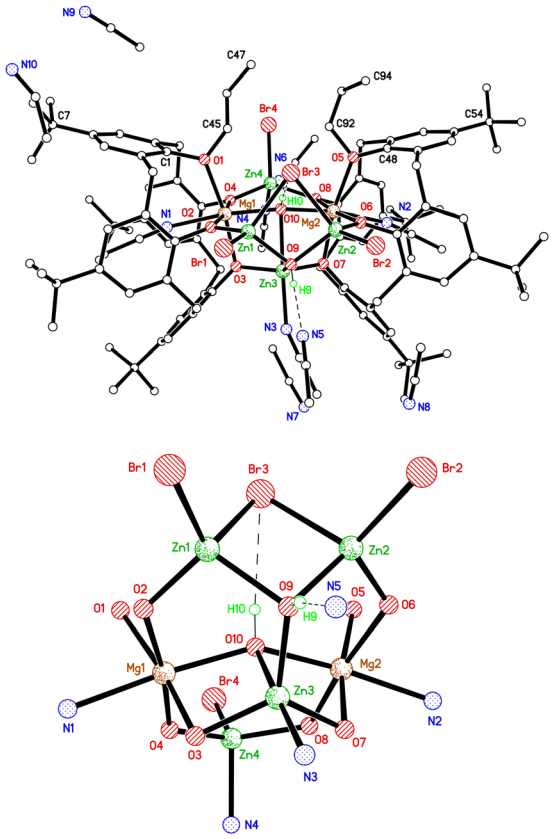

Fig. 2 (top) Molecular structure of [(ZnBr(NCMe)][Br/ClZn(μ-Br/cl)ZnBr/Cl](μ^3-OH)$_2$[Mg(MeCN)L(O*n*-Pr)]$_2$·5.19MeCN (**2**·5.19MeCN); (bottom) view of the core of **2**·5.19MeCN. Selected bond lengths (Å) and angles (°): Mg(1)–O(1) 2.156(3), Mg(1)–O(2) 2.101(3), Mg(1)–O(3) 2.006(3), Mg(1)–O(4) 2.040(3), Mg(1)–O(10) 2.088(3), Mg(1)–N(1) 2.225(3), Zn(1)–O(2) 1.930(3), Zn(1)–O(9) 2.030(3), Zn(1)–Br(1) 2.3097(7), Zn(1)–Br(3) 2.4812(8), Zn(3)–O(3) 1.933(2), Zn(3)–O(7) 1.947(3), Zn(3)–O(9) 2.033(3), Zn(3)–O(10) 2.265(3), Zn(3)–N(3) 2.115(4), O(1)–Mg(1)–O(2) 86.56(11), N(1)–Mg(1)–O(3) 87.82(12), N(1)–Mg(1)–O(10) 172.29(14), Mg(1)–O(2)–Zn(1) 124.39(13), Zn(1)–O(9)–Zn(2) 96.29(12), Zn(1)–Br(3)–Zn(2) 74.53(3), O(3)–Zn(3)–O(7) 113.36(11), Mg(1)–O(3)–Zn(3) 100.20(11), Mg(2)–O(7)–Zn(3) 101.62(12). Most H atoms and minor disorder components omitted.

On slightly varying the conditions by employing toluene when adding Br_2Zn, the product $\{[ZnX(NCMe)]_3[Mg(NCMe)]_2[Mg(NCMe)_2](OH)_2(L)(LH)\}\cdot 4MeCN$ (**3**·4MeCN) {X = $Br_{0.84}Cl_{0.16}$} was isolated from a saturated MeCN solution at 0 °C. The molecular structure is shown in Fig. 3 with selected bond lengths and angles given in the caption. The molecule lies on a mirror plane, so half is unique. The structure contains 2 unique Mg^{2+} ions with Mg(1) adopting an octahedral geometry and coordinates to 5 oxygens (4 from a calixarene plus a hydroxo) and an MeCN, whilst Mg(2) is closer to square-based pyramidal (τ = 0.33),[13] and coordinates to 3 oxygens (2 calixarene and a hydroxy centre) and 2 NCMe ligands. There are also 2 unique, tetrahedral Zn^{2+} ions which both coordinate to a X^-; Zn(2) also coordinates to an MeCN and a hydroxy, while Zn(1) also coordinates to a second calixarene oxygen and an MeCN. H-bonding occurs between two calixarene oxygens, one from each identical half of the complex, so the H was modelled as located on the mirror plane with O(4)···H(4) = 1.214(7) Å.

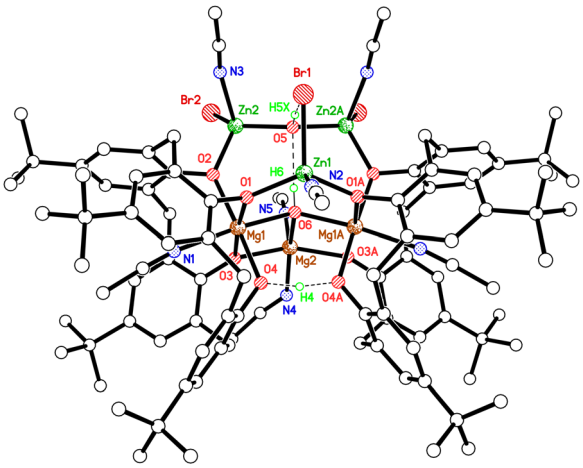

Fig. 3 Molecular structure of {[ZnX(NCMe)]$_3$[Mg(NCMe)]$_2$[Mg(NCMe)$_2$](OH)$_2$(L)(LH)}·4MeCN (**3**·4MeCN) {X = $Br_{0.84}Cl_{0.16}$}; selected bond lengths (Å) and angles (°): Mg(1)–O(1) 2.032(3), Mg(1)–O(2) 2.041(3), Mg(1)–O(3) 2.031(3), Mg(1)–O(4) 2.010(3), Mg(1)–O(6) 1.9882(17), Mg(1)–N(1) 2.182(3), Mg(2)–O(3) 1.964(2), Mg(2)–O(6) 2.102(4), Mg(2)–N(4) 2.132(8), Mg(2)–N(5) 1.946(10), Zn(1)–O(1) 1.948(2), Zn(1)–N(2) 2.070(5), Zn(1)–Br(1) 2.3829(10), Zn(2)–O(2) 1.964(3), Zn(2)–O(5) 1.922(2), Zn(2)–Br(2) 2.2863(10), Zn(2)–N(3) 2.088(6); O(1)–Mg(1)–O(2) 91.46(12), O(1)–Mg(1)–O(3) 174.99(11), N(1)–Mg(1)–O(6) 173.04(14), O(6)–Mg(2)–N(5) 111.7(4), O(3)–Mg(2)–O(3A) 142.08(19), O(1)–Zn(1)–O(1A) 120.92(14), Br(1)–Zn(1)–N(2) 103.88(13), O(2)–Zn(2)–O(5) 101.40(18), Zn(2)–O(5)–Zn(2A) 139.9(3). Most H atoms & minor disorder components omitted.

Overall, there is a central cage structure involving all the metal ions bridged by oxygens (Fig. S5, ESI†). The charges from the 6 M^{2+} ions are off-set by one 3− calixarene (one shared residual proton), the second 4-calixarene, 2 × OH^-, and 3 × Br^-.

Similar use of L(O*n*-Pentyl)$_3$H led, following work-up (MeCN), to the complex [$Mg_5Zn_2(OH)_4(LH_2)_2$(LOPentyl)$_2$(NCMe)$_2$]·5MeCN (**4**·5MeCN). Crystals isolated consistently suffered from severe twinning which could not be resolved. However, the connectivity is clearly established (Fig. 4 and Fig. S7 ESI†). In terms of charge, there are 14 negative charges generated from 2 × L(Opentyl) (6−), 2 × LH_2 (4−), 4 × OH^- (4−), which is balanced by 7 × M^{2+} ions. The centres Mg(1), Mg(3), & Mg(5) are octahedral, while both Mg(2) and Mg(4) are 5-coordinate; Mg(4) additionally makes a short contact with a CH_2 H atom H(53X) at 2.17 Å. Both Zn^{2+} ions are considerably distorted tetrahedral with Zn(1) additionally making a short contact with H(17B) at 2.10 Å and Zn(2) making a similar contact with H(82A) at 2.19 Å; both of these H atoms are from calixarene CH_2 groups. Both Mg(1) and Mg(3) are coordinated to NCMe ligands as well as calixarene O atoms and OH^-. One calixarene bonds only to Mg(1) and bears a pentyl group and has an NCMe ligand bound to Mg(1) in the cavity and a hydroxy group *trans* to that. A second calixarene bridges the centres Mg(2) and Zn(2), whilst a third calixarene is similar to the Mg(1) bound calixarene, but at Mg(3). A fourth calixarene is similar to the second calixarene, but bridging Mg(4) and Zn(1). The residual protons on the 2nd and 4th calixarenes bridge to a neighbouring phenolate O. Two hydroxy groups cap three Mg^{2+} ions, while the other two cap two Mg^{2+} ions and one Zn^{2+} ion.

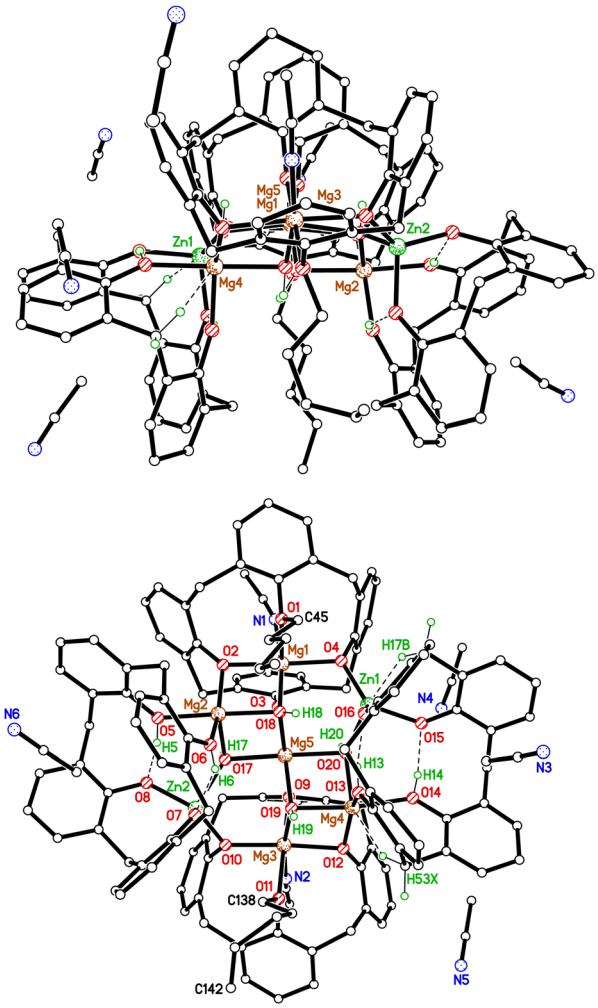

Fig. 4 Two views of the molecular structure of [$Mg_5Zn_2(OH)_4(LH_2)_2$-(LOpentyl)$_2$(NCMe)$_2$]·5MeCN **4**·5MeCN (*tert*-butyl groups & most H atoms omitted for clarity). Selected bond lengths (Å) and angles (°): Mg(1)–O(1) 2.141(17), Mg–(non-alkylated calixarene O) range 1.937–2.073(17), Mg(1)–O(18) 2.033(15), Mg(1)–N(1) 2.20(2), Mg(2)–O(17) 1.994(15), Mg(2)–O(18) 2.053(13), Mg(5)–O(17) 2.081(15), Mg(5)–O(18) 2.145(14), Mg(5)–O(19) 2.114(16), Mg(5)–O(20) 2.083(17), Zn–(non-alkylated calixarene O) range 1.862–1.935(18), Zn(1)–O(20) 1.981(15); Mg(1)–O(2)–Mg(2) 97.5(7), Mg(1)–O(18)–Mg(5) 98.0(7), Mg(2)–O(17)–Mg(5) 97.6(7), Mg(3)–O(12)–Mg(4) 98.6(6), Mg(3)–O(9)–Mg(5) 101.7(9), Mg(2)–O(17)–Zn(2) 120.7(8), Mg(3)–O(10)–Zn(2) 119.3(8), Mg(4)–O(19)–Mg(5) 94.6(6), Mg(1)–O(4)–Zn(1) 114.0(7).

In the core of the molecule there are two apically vacant Mg_3O_4 cubes connected by an apex at Mg(5), see Fig. S8, ESI.†

Complexes **1–4** have been screened for their potential to act as catalysts for the ROP of ε-caprolactone (ε-CL), with and without benzyl alcohol (BnOH) present. Using **1** and **2**, the ratio [CL]:[**cat**]:[BnOH], time, and temperature were varied, see Table S2, ESI.† At ambient temperature, using a ratio of 500 : 1 : 2 ([CL]:[**cat**]:BnOH), the systems were inactive. Only on elevating the temperature (130 °C) was appreciable conversion observed over 24 h. For example, [500]:[**1**]:2BnOH afforded 82% conversion in the presence of 2 equivalents of BnOH under N_2. The ^{1}H NMR spectrum of the PCL formed in the presence of BnOH indicated the presence of a BnO end group (*e.g.* Fig. S10, ESI†),

whilst the MALDI-ToF M.S. (Fig. S11, ESI†) shows a low mass series assigned to the sodium exchange artefact where the carboxylic proton has exchanged for Na, and a higher mass series assigned to BnO–/–OMe terminated polymers. For **2**, the MALDI-ToF M.S. indicated the presence of chain polymers terminated by OH (Fig. S12, ESI†). Prolonging the time to 72 h generally led to multimodal behaviour (entries 4, 12, 21, Table S2, ESI†). Conducting runs without BnOH or under air tended to lead to lower conversions. For complexes **3** and **4** (using the ratio [500] : [1] : [2]), good conversion was again only achieved at 130 °C. Over 24 and 72 h, complex **3** performed less well *versus* **4**, with quantitative conversion observed for the latter over 72 h.

Kinetic studies (Fig. S15, ESI†), conducted using 500 : 1 : 2 ([CL] : [**cat**] : [BnOH]) revealed the rate trend **1** ≈ **4** < **3** ≫ **2**, together with the absence of an induction period and first-order kinetics with respect to monomer. For comparative purposes, known complexes [(*n*BuMg)L(O*n*Pr)$_2$] (**I**) and [Zn$_3$(OH)$_2$L(Opentyl)$_2$] (**II**) (Fig. S9, ESI†) were screened herein under similar conditions.[14] Results reveal that **I** exhibits poor conversion of ε-CL at 130 °C, most likely due to thermal instability. Meanwhile, **II** can achieve high conversion at 90 °C, albeit with less control. Given metal-free catalysts are also known,[15] calixarenes L(OMe)$_2$H$_2$ and L(O*n*-pentyl)$_3$H were screened under similar conditions (entries 34 and 35, Table S2, ESI†); little or no conversion was observed.

The complexes were examined for their ROP potential under solvent-free conditions (Table S3, ESI†). Results were better with BnOH present, whilst the systems tended to exhibit bi-modal behaviour. Best conversion was achieved using **1**, albeit with poorer control. From the MALDI-ToF M.S. (Fig. S16 and S17, ESI†), it was evident that several PCL series were present (as Na adducts). For **1**/2BnOH, the main family can be identified as bearing BnO–/–H end groups, whilst in the absence of BnOH, a HO–/–H (and a +3 Da offset series overlapping) family is evident.

Finally, the complexes were evaluated for ROP of ε-CL as melts under air in the presence of BnOH. In general, lower conversions were achieved *versus* N_2, although for **1** the resulting polymer exhibited a higher molecular weight (M_n) than that formed under N_2.

For several entries, both in solution and as melts, molecular weights obtained *via* gpc were not in good agreement with calculated values. Moreover, $Đ_s$ were in the range 1.09 to 1.60 in solution and 1.10–1.84 as melts, which suggests that these mixed Mg/Zn systems contain multiple active species and/or transesterification processes occurred. We propose similar processes operate here as reported for metallocalixarene ROP catalysts involving two-site chain growth.[16]

Comparison of **1–4** with systems screened under related conditions (*i.e.*, same laboratory) revealed that they outperform Sc or Ti-based calixarenes in terms of conversion and polymer M_n. They are comparable with Zn, Nb, or Ta-based calixarenes; the Zn-based systems afford similar high M_n products. A mixed Co/Zn Schiff-base macrocycle exhibited comparable conversions to **1–4**, but lower M_n products; homo Co/Zn analogues were inactive. An aminobis(phenolate) trinuclear complex outperforms **1–4** with better conversion at 90 °C. For these comparisons and others, see Table S4 (ESI†).

In conclusion, we have structurally characterised a number of rare examples of mixed-metal calix[4]arenes using organomagnesium and organozinc or zinc bromide as entry points. A number of unusual structures were identified, particularly when employing the tris(pentoxy)calix[4]arene as starting material. The products are capable of the efficient ROP of ε-CL at 130 °C over 24 h, affording mixtures of low and high molecular weight products with differing end groups.

We are now investigating the ability of calix[4]arenes to accommodate other mixed-metal systems of catalytic interest.

CR thanks the EPSRC (grant EP/S025537/1) and the EPSRC National Crystallography Service, Southampton for data collection.

Conflicts of interest

There are no conflicts to declare.

References

1 See for example, N. Singh, O. A. Ogunseitan, M. H. Wong and Y. Tang, *Sustainable Horiz.*, 2022, **2**, 100016.
2 For reviews, see (*a*) B. J. O'Keefe, M. A. Hillmeyer and W. B. Tolman, *J. Chem. Soc., Dalton Trans.*, 2001, 2215–2224; O. Dechy-Cabaret, B. Martin-Vaca and D. Bourissou, *Chem. Rev.*, 2004, **104**, 6147–6176; (*b*) M. Labet and W. Thielemans, *Chem. Soc. Rev.*, 2009, **38**, 3484–3504; (*c*) C. M. Thomas, *Chem. Soc. Rev.*, 2010, **39**, 165–173; (*d*) A. Arbaoui and C. Redshaw, *Polym. Chem.*, 2010, **1**, 801–826; (*e*) A. P. Dove, *ACS Macro Lett.*, 2012, **1**(1409), 1412; (*f*) Y. Sarazin and J.-F. Carpentier, *Chem. Rev.*, 2015, **115**, 3564–3614; (*g*) J. Gao, D. Zhu, W. Zhang, G. A. Solan, Y. Ma and W.-H. Sun, *Inorg. Chem. Front.*, 2019, **6**, 2619–2652; (*h*) E. Tazekas, P. A. Lowy, M. A. Rahman, A. Lykkeberg, Y. Zhou, R. Chambenahalli and J. A. Garden, *Chem. Soc. Rev.*, 2022, **51**, 8793–8814.
3 (*a*) D. H. Homden and C. Redshaw, *Chem. Rev.*, 2008, **108**, 5086–5130; (*b*) O. Santoro and C. Redshaw, *Coord. Chem. Rev.*, 2021, **448**, 214173.
4 C. Redshaw, M. R. J. Elsegood, J. A. Wright, H. Baillie-Johnson, T. Yamato, S. De Giovanni and A. Mueller, *Chem. Commun.*, 2012, **48**, 1129–1131.
5 C. Redshaw, *Coord. Chem. Rev.*, 2003, **244**, 45–70.
6 L. R. B. Wilson, M. Coletta, M. Evangelista, S. Piligkos, S. J. Dalgarno and E. K. Brechin, *Dalton Trans.*, 2022, **51**, 4213–4226.
7 (*a*) S. Sanz, K. Ferreira, R. D. McIntosh, S. J. Dalgarno and E. K. Brechin, *Chem. Commun.*, 2011, **47**, 9042–9044; (*b*) T. Kajiwara, R. Shinagawa, T. Ito, N. Kon, N. Iki and S. Miyano, *Bull. Chem. Soc. Jpn.*, 2003, **76**, 2267–2275; (*c*) T. Xing, M. Derbyshire, M. R. J. Elsegood and C. Redshaw, *Chem. Commun.*, 2022, **58**, 7427–7430.
8 W. Gruszka and J. A. Garden, *Nat. Commun.*, 2021, **12**, 3252.
9 (*a*) J. D. Ryan, K. J. Gagnon, S. J. Teat and R. D. McIntosh, *Chem. Commun.*, 2016, **52**, 9071–9073; (*b*) L.-J. Wu, W. Lee, P. K. Ganta, Y.-L. Chang, Y.-C. Chang and H.-Y. Chan, *Coord. Chem. Rev.*, 2023, **475**, 214847.
10 For lactide see: G. Sachdeva, Y. Bamal, A. Ladan, O. S. Tiwari, V. Rawat, P. Yadav and V. P. Verma, *ACS Omega*, 2023, **8**, 13479–13491.
11 E. Martin, D. L. Hughes, M. B. Hursthouse, L. Male and S. J. Lancaster, *Dalton Trans.*, 2009, 1593–1661.
12 K. Wang, T. J. Prior and C. Redshaw, *Chem. Commun.*, 2019, **55**, 11279–11282.
13 A. W. Addison, T. N. Rao, J. Reedijk, J. van Rijn and G. C. Verschoor, *J. Chem. Soc., Dalton Trans.*, 1984, 1349–1356.
14 (*a*) M. J. Walton, S. J. Lancaster and C. Redshaw, *ChemCatChem*, 2014, **6**, 1892–1898; (*b*) T. Xing, J. W. A. Frese, M. Derbyshire, M. A. Glenister, M. R. J. Elsegood and C. Redshaw, *Dalton Trans.*, 2022, **51**, 11776–11786.
15 A. P. Dove, *ACS Macro Lett.*, 2012, **1**, 1409–1412.
16 Z. Sun, Y. Zhao, O. Santoro, M. R. J. Elsegood, E. V. Bedwell, K. Zahra, A. Walton and C. Redshaw, *Catal. Sci. Tech.*, 2020, **10**, 1619–1639.